

Histopathological, ultrastructural, and biochemical traits of apoptosis induced by peroxisomicine A1 (toxin T-514) from *Karwinskia parvifolia* in kidney and lung

Adolfo Soto-Domínguez^{a,1}, Daniel Salas-Treviño^{a,1}, Gloria A. Guillén-Meléndez^a, Uziel Castillo-Velázquez^b, Raquel G. Ballesteros-Elizondo^a, Carlos R. Montes-de-Oca-Saucedo^a, Sheila A. Villa-Cedillo^a, Rodolfo Morales-Ávalos^c, Luis E. Rodríguez-Tovar^b, Roberto Montes-de-Oca-Luna^a, Odila Saucedo-Cárdenas^{a,*}

^a Universidad Autónoma de Nuevo León, Facultad de Medicina, Departamento de Histología, Av. Madero y E. Aguirre-Pequeño s/n, Col. Mitras Centro, Monterrey, N.L., C.P. 64460, Mexico

^b Universidad Autónoma de Nuevo León, Facultad de Medicina Veterinaria y Zootecnia, Cuerpo Académico de Zoonosis y Enfermedades Emergentes. General Escobedo, N. L., C.P. 66050, Mexico

^c Universidad Autónoma de Nuevo León. Facultad de Medicina, Departamento de Fisiología. Av. Madero y E. Aguirre-Pequeño s/n, Col. Mitras Centro, Monterrey, N.L., C. P. 64460, Mexico

ARTICLE INFO

Handling Editor: Ray Norton

Keywords:

Peroxisomicine A1
Apoptosis
Necrosis
Mitochondria
Kidney and Lung intoxication
Plant toxin

ABSTRACT

Peroxisomicine A1 (PA1) is a toxin isolated from the *Karwinskia* genus plants whose target organs are the liver, kidney, and lung. *In vitro* studies demonstrated the induction of apoptosis by PA1 in cancer cell lines, and *in vivo* in the liver. Apoptosis has a wide range of morphological features such as cell shrinkage, plasma membrane blistering, loss of microvilli, cytoplasm, and chromatin condensation, internucleosomal DNA fragmentation, and formation of apoptotic bodies that are phagocytized by resident macrophages or nearby cells. Early stages of apoptosis can be detected by mitochondrial alterations. We investigated the presence of apoptosis *in vivo* at the morphological, ultrastructural, and biochemical levels in two target organs of PA1: kidney and lung. Sixty CD-1 mice were divided into three groups (n = 20): untreated control (ST), vehicle control (VH), and PA1 intoxicated group (2LD50). Five animals of each group were sacrificed at 4, 8, 12, and 24 h post-intoxication. Kidney and lung were examined by morphometry, histopathology, ultrastructural, and DNA fragmentation analysis. Pre-apoptotic mitochondrial alterations were present at 4 h. Apoptotic bodies were observed at 8 h and increased over time. TUNEL positive cells were detected as early as 4 h, and the DNA ladder pattern was observed at 12 h and 24 h. The liver showed the highest value of fragmented DNA, followed by the kidney and the lung. We demonstrated the induction of apoptosis by a toxic dose of PA1 in the kidney and lung *in vivo*. These results could be useful in understanding the mechanism of action of this compound at toxic doses *in vivo*.

1. Introduction

Peroxisomicine A1 (T-514) is a toxin isolated from the endocarp of *Karwinskia humboldtiana* (Dreyer et al., 1975), whose target organs are the liver, kidney, and lung (Bermúdez et al., 1986; Bermúdez et al., 1992). Piñeyro et al. in 1994 described for the first time *in vitro* selective toxicity of T-514 on human tumor cell lines of liver, lung, and colon, suggesting the use of T-514 as a potential antineoplastic agent (Piñeyro

et al., 1994). Studies performed in methylotrophic yeasts showed that T-514 causes selective and irreversible damage to peroxisomes engulfed by macropexophagy at non-lethal doses, leading to T-514 being renamed Peroxisomicine A1 (PA1) (Sepulveda Saavedra et al., 1992). Recently it was demonstrated that PA1 also causes micropexophagy in *C. boidinii* (Ortega-Martínez et al., 2020).

In vitro studies showed that PA1 has an apoptotic effect in human leukemia cells (Lansiaux et al., 2001), HeLa cells, human breast

* Corresponding author. Departamento de Histología Facultad de Medicina, UANL, Monterrey, N.L., 64460, Mexico.

E-mail address: odila.saucedocr@uanl.edu.mx (O. Saucedo-Cárdenas).

¹ Contributed equally.

adenocarcinoma, colon adenocarcinoma, and hepatoma lines (Martínez et al., 2001). In an *in vivo* study, our work group demonstrated that early intraperitoneal (i.p.) therapy, administration of PA1 (1 mg/kg), caused necrosis of tumor TC-1 cells implanted in C57BL/6 mice without affecting the liver, kidney, or lung (Soto-Domínguez et al., 2012). However, in a recent *in vivo* study using an elevated dose of PA1 to simulate an acute intoxication (28 mg/kg), we observed prominent cell death in the liver, triggered by the intrinsic apoptotic pathway (Soto-Domínguez et al., 2018).

Morphological characteristics of cell death by apoptosis differ from the characteristics shown by necrosis (Kerr et al., 1972). In tissues, the changes that occur in apoptosis or necrosis are different (Majno and Joris, 1995). Necrosis causes cell death due to direct physical or chemical damage that usually begins on the surface of the cell, followed by swelling of the cell and pyknosis. Afterwards, early lysis occurs, and there is an uncontrolled release of proteolytic enzymes from the cytoplasm, caused by the rupture of the plasmalemma, which triggers an inflammatory process (Kerr et al., 1995). In contrast, in apoptosis cells show shrinkage, formation of bubbles or blisters on the cell surface, chromatin is condensed in thick masses, internucleosome segmentation occurs, and apoptotic bodies (cell fragments surrounded by a membrane) are finally produced, thus preventing the release of intracellular contents. Within tissues, apoptotic bodies are rapidly phagocytized by resident macrophages or by neighboring cells, including epithelial cells (Kerr, 1994).

Ultrastructural studies have reported pre-apoptotic changes in mitochondria before chromatin fragmentation; these changes consist of herniation of the inner membrane through the rupture of the outer membrane with focal swelling of the matrix and unfolding of the nearby crests (Soto-Domínguez et al., 2018; Angermüller et al., 1998). On the other hand, necrosis leads to mitochondria swelling, moderate crest reduction, and partial or total loss of the mitochondrial matrix. In this study, we investigated the *in vivo* toxic effects of PA1 in kidney and lung, additional target organs of this toxin, using the acute dose of 28 mg/kg.

2. Materials and methods

2.1. Study groups

We used 60 CD-1 male young mice (5–6 weeks old, weight: 30–35 g), maintained with a standard laboratory diet and water *ad libitum*. The mice were randomly divided into three groups ($n = 20$): Untreated (ST), Vehicle (VH), and Intoxicated (PA1) with a single dose of PA1 ($2LD_{50} = 28$ mg/kg) dissolved in commercial safflower oil as the vehicle and administered via i. p. Mice intoxicated with this dose had a 100% mortality at 48 h post-treatment (Soto-Domínguez et al., 2018).

All experiments were performed according to the International Guidelines on the Appropriate Use of Experimental Animals and to the Mexican current legislation on lab animals (NOM-062-ZOO-1999). PA1 was obtained from the seeds of *K. parvifolia*, and the isolation, purification, and evaluation process were performed based on previously described standards (Guerrero et al., 1987; Waksman and Ramírez, 1992).

2.2. Sample collection

Five animals from each group (ST, VH, PA1) were euthanized at 4, 8, 12, and 24 h post-treatment. Kidneys and lungs were collected and divided into three fractions to perform morphological analysis with light microscopy, ultrastructural analysis by transmission electron microscopy (TEM), and biochemical analysis. Liver samples were also collected for the fragmented DNA spectrophotometric quantization.

2.3. Morphological analysis

2.3.1. Analysis by light microscopy

Lungs and kidney samples were fixed for 24 h with 4% buffered (PBS 1X, pH: 7.2–7.4) paraformaldehyde (PFA), and subsequently processed to obtain paraffin-embedded tissue blocks. Histological sections of 5 μ m were stained with Hematoxylin and Eosin (H&E), and Masson Trichrome (MT). Tissues were analyzed for distinctive morphological findings of apoptotic processes, such as nuclear fragmentation, condensed chromatin, and loss or condensation of the cytoplasm. Digital high-resolution images were obtained with a Nikon Microscope Eclipse 50i with the Q-Capture Pro image analysis system. All the analyses were evaluated by three-blinded independent experts in morphology.

2.3.2. Immunohistochemistry for chromatin fragmentation using TUNEL

TUNEL technique was performed with the TACS™ 2 TdT DAB *In Situ* Apoptosis Detection kit from Trevigen® (Gaithersburg, Md; USA) in 6 μ m lung and kidney histological sections. Control slices were prepared according to the specifications of the kit: incubation with nuclease to induce DNA fragmentation (positive control) or omitting the labeling enzyme (negative control). The tissues were analyzed by light microscopy, and microphotographs were taken with a Nikon Microscope Eclipse 50i with the Q-Capture Pro image analysis system. A morphometric analysis was performed to quantify TUNEL-positive cells/field; this was performed in 24 random fields per group (eight fields/slide, one slide/mouse, three mice/group). These were studied with an oil immersion objective (100 \times), and quantification was performed in triplicate in kidneys and lungs of all the study groups.

2.3.3. Ultrastructural analysis by transmission electron microscopy

In ultrastructural analysis, samples were fixed in Karnovsky-Ito solution (4% PFA, 5% glutaraldehyde, and 0.05% picric acid in cacodylates buffer with pH: 7.2–7.4) (Ito, 1968) during 24 h at room temperature (RT). For post-fixation we used 2% aqueous osmium tetroxide for 1 h; samples were then treated with a 1% aqueous solution of uranyl nitrate. After rapid dehydration with 30%–100% gradual acetone, tissues were embedded in epoxy resin. Sectioning was done with a diamond knife on an RMC ultramicrotome. Semithin 350 nm thick sections were stained with 1% toluidine blue (TB) for the study of apoptotic and/or necrotic features with a light microscope. Also, ultra-thin (70 nm) sections were collected on 200-mesh copper grids without a supportive substrate. Sections were counterstained with uranyl acetate and lead citrate and analyzed on a Carl Zeiss EM109 electron microscope.

2.4. Biochemical analysis

2.4.1. Detection of DNA fragmentation in agarose gels

Portions of lung and kidney collected samples were stored at -80°C until their biochemical evaluation of DNA fragmentation was performed, with a method described by Guan et al. (2002). Samples were thawed and kept on ice; subsequently, samples were immersed in cold buffer (50 mmol/L phosphates, 120 mmol/L NaCl, and 10 mmol/L EDTA, pH7.4) in a ratio of 1:3 and were homogenized with intervals of 10 s in buffer and 5 s on ice (10 times). Then the samples were centrifuged at 27,000 g at 4°C for 20 min. The supernatant was collected and treated with RNase (200 $\mu\text{g}/\text{mL}$) for 30 min at 37°C and the DNA was extracted by phenol-chloroform. DNA was resuspended in TE 1 X buffer (10 mmol/L Tris-HCl, pH 8.0, and 1 mmol/L EDTA), and mixed with loading buffer to analyze the samples by electrophoresis in 1.8% agarose gel using ethidium bromide. The same amount of DNA was loaded for each of the analyzed groups.

2.4.2. Quantization of fragmented DNA by spectrophotometry

The spectrophotometric quantization of fragmented DNA was performed according to the method described by Burton (1956) and

modified by Guan et al. (2002). Following this, the 27,000 g supernatant (fragmented soluble DNA), and the pellet (genomic DNA) were collected. Afterwards, perchloric acid was added to a final concentration of 0.5 N and samples were hydrolyzed at 70 °C for 70 min; then, samples were cooled at 4 °C for 5 min and centrifuged for 6 min (4000 g) at 4 °C to remove the protein. The supernatant was collected, and DNA content was determined by the diphenylamine reaction as reported previously (Gendimenico et al., 1988). This technique was used in the kidney and

lung samples of the group intoxicated with PA1 at 24 h. Additionally, we included liver samples from our previous report to compare them with lung and kidney samples of the current study, since this evaluation was not performed (Soto-Domínguez et al., 2018). The quantization of fragmented DNA by spectrophotometry was performed in triplicate, and the data was subjected to statistical analysis with a one-way ANOVA test to evaluate the degree of induction of apoptosis present in the studied organs.

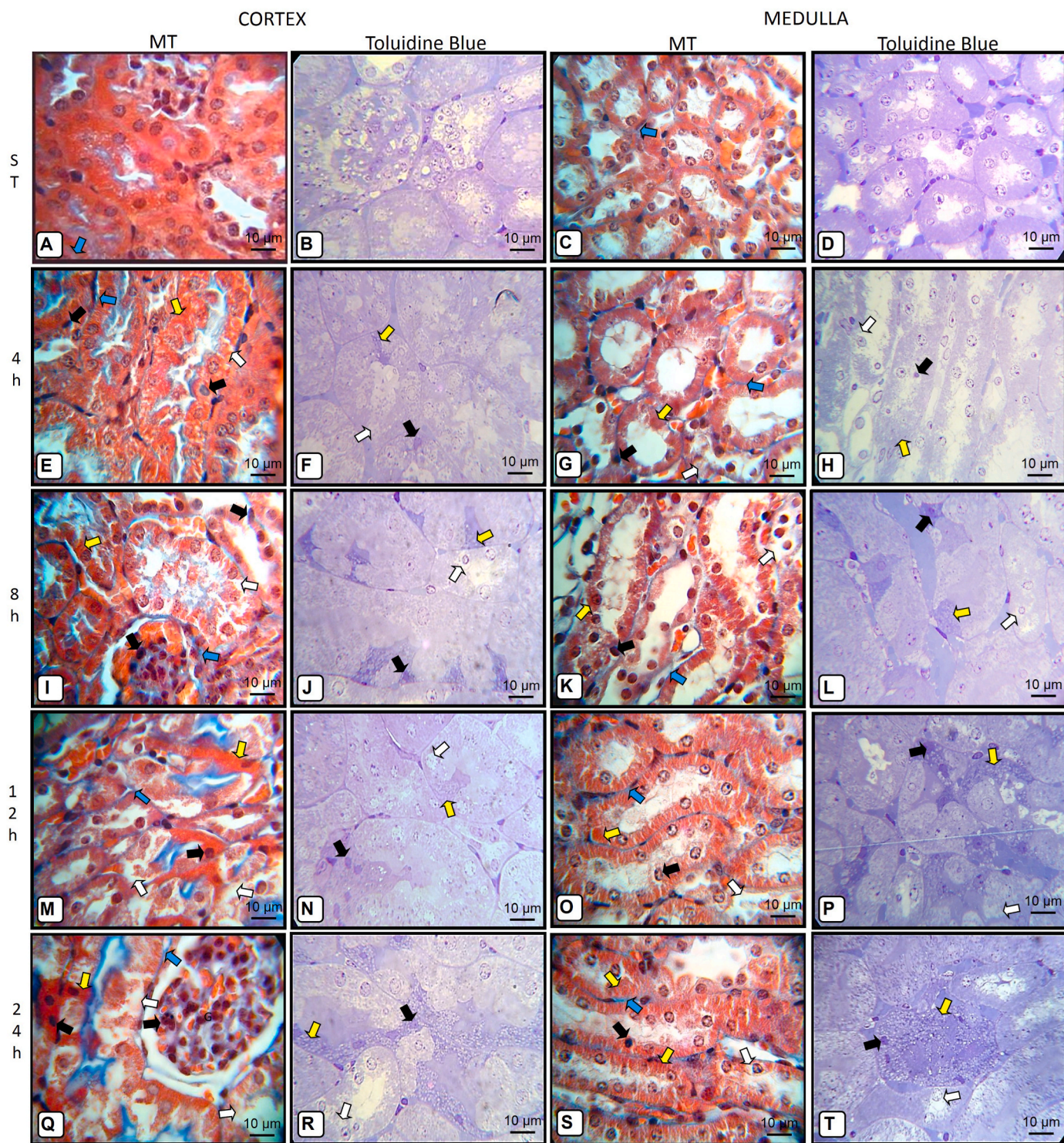


Fig. 1. Morphological apoptotic and necrotic damage in the kidney. Non-treated group (A–D) without damage in cortex and medulla. Kidneys of PA1 intoxicated mice at 4 h (E–H); 8 h (I–L); 12 h (M–P); 24 h (Q–T) showing nuclei with condensed chromatin (black arrows), condensed cytoplasm (yellow arrows), loss of cytoplasm (white arrows), collagen fibers (blue arrows). Scale 10 μm.

3. Results

3.1. PA1 induces apoptotic and necrotic histological alterations in kidney

The histological changes that occur in apoptotic processes are usually variable, depending on the type of tissue, and in particular, the

affected cells. To describe these changes in renal tissue, we analyzed the histological structure of the samples treated with PA1. We found that kidney samples showed normal histology in the non-treated and VH control groups: cortex and medulla structures showed tissue integrity and structure, with neither signs of inflammation nor edema (Fig. 1A–D).

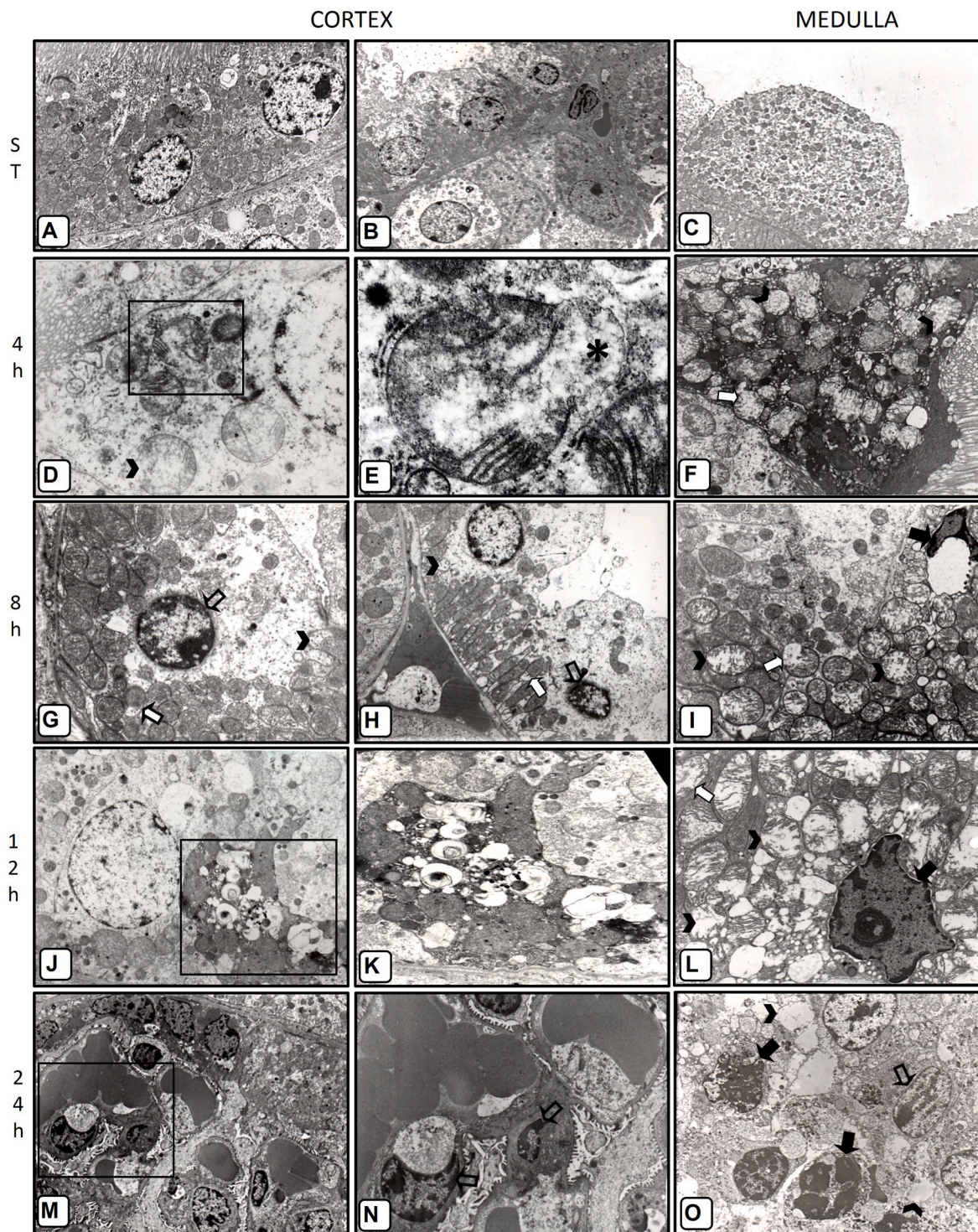


Fig. 2. Ultrastructural apoptotic and necrotic damage alterations in the kidney. Renal cortex of non-treated mice, cells of proximal (A) and distal convoluted (B) tubules without alterations. C) Collector tubule of the renal medulla with its normal ultrastructure. Kidneys of PA1 intoxicated mice at 4 h (D, E, F); 8 h (G, H, I); 12 h (J, K, L); 24 h (M, N, O) showing mitochondria with pre-apoptotic alterations (white arrows): rupture of outer mitochondrial membrane (*), nuclei with condensed chromatin (empty arrows), necrotic mitochondria with alterations like loss of mitochondrial matrix (arrow heads), pyknotic nuclei (black arrows), J and K show apoptotic bodies. Microphotographs magnification: A, D, G, J, M: 2000×; B:2500X; C, K, N:4000X; L: 6300X, E:10000X.

At 4 h PA1 post-intoxication, the kidney began to show interesting alterations compatible with apoptosis such as chromatin and cytoplasm condensation, and variable nuclei sizes in the epithelial cells of the renal cortex (Fig. 1E and F), and medulla (Fig. 1G and H); these alterations increased after 8 h of PA1 in both areas (Fig. 1I - L).

In the mice intoxicated with PA1 at 12 h, chromatin condensation of the tubular epithelial cells, and generalized areas of necrosis were observed; moreover, the presence of collagen fibers increased in the cortex (Fig. 1M and N) and renal medulla (Fig. 1O and P). Finally, at 24 h post-intoxication, the presence of apoptotic bodies, collagen fibers and necrosis signs were increased. Apoptotic bodies were observed in the

intraglomerular mesangial cells, and in the epithelial cells of the proximal convoluted tubule (PCT), distal convoluted tubule (DCT), collector tubule (CT), and loop of Henle (LH) of the renal cortex and medulla (Fig. 1Q-T).

3.2. PA1 induces pre-apoptotic and necrotic mitochondrial alterations in kidney tissue

The renal cortex and medulla were analyzed by TEM to identify the presence of mitochondrial alterations corresponding to pre-apoptotic signs (Angermüller et al., 1988). In the ST non-treated group,

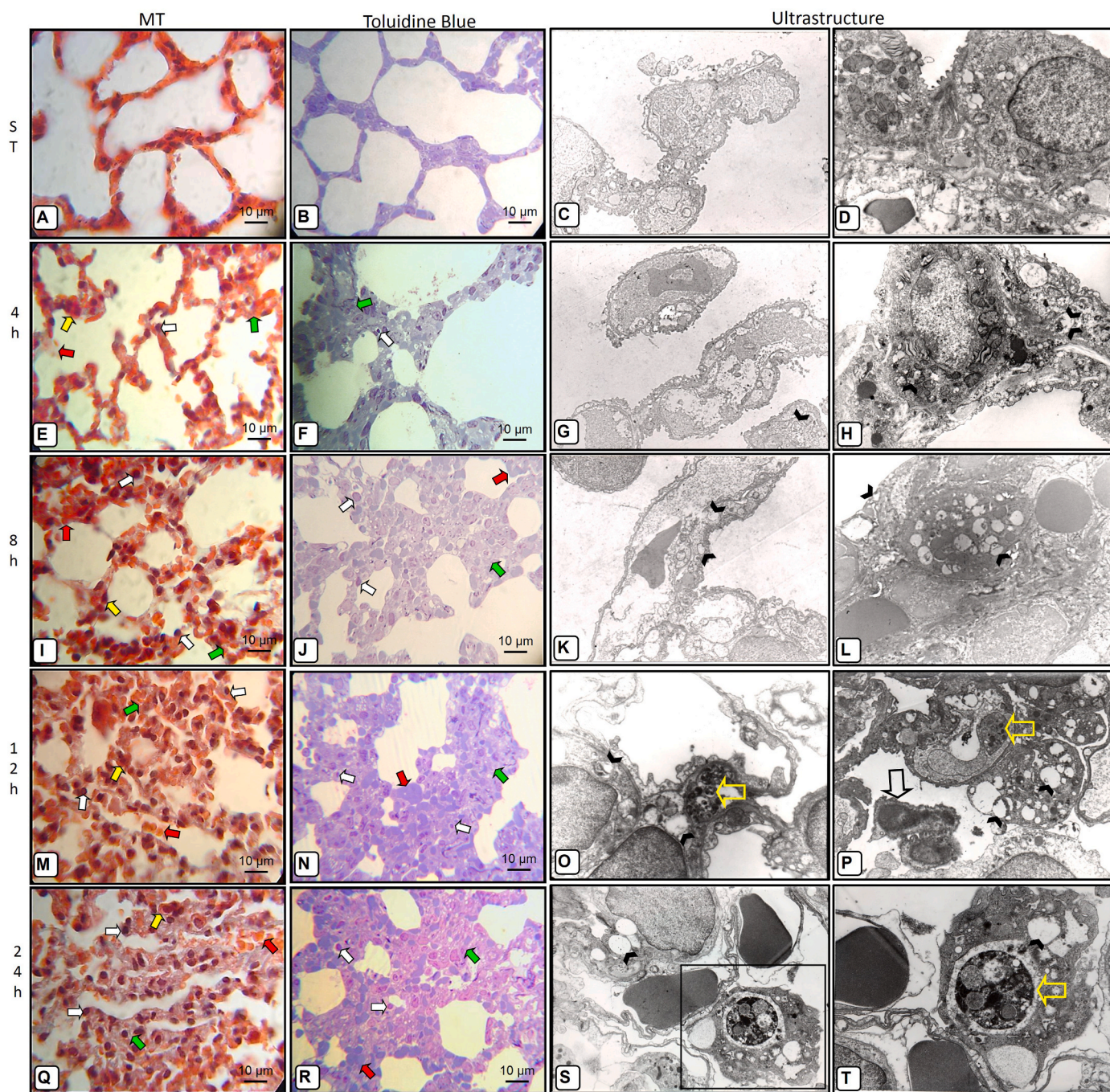


Fig. 3. Apoptotic damage by PA1 in the lung. Lungs of the non-treated group without histological (A, B) or ultrastructural (C, D) signs of apoptosis. Lungs of mice treated 4 h after PA1 administration (E-H), 8 h (I-L), 12 h (M-P), and 24 h (Q-T). Condensed chromatin (white arrows), condensed cytoplasm (yellow arrows), thickening of interalveolar septa (green arrows), hemorrhage (red arrows), mitochondria with pre-apoptotic alterations (arrow heads), apoptotic bodies (empty yellow arrows). T) is a magnification of the black box area in S. Magnifications: A, B, E, F, I, J, M, N, Q, R: Scale 10 µm; C, D, G, K, O, S: 4400X; D, H, L, P, T: 6300X.

mitochondria of the renal cortex and medulla cells show integral morphology (Fig. 2A–C). At 4 h after treatment with PA1, the renal cells showed mitochondria with pre-apoptotic alterations such as localized rupture of the outer membrane, blistering of the inner membrane with focal swelling of the matrix, and loss of cristae in the zone of the breach of the outer membrane. At the same time, mitochondria with signs of necrosis were observed: increase in mitochondrial size, and loss of the matrix with unfolding of the cristae (Fig. 2D and E).

3.3. Ultrastructural characteristics of apoptosis induced by PA1 in kidney

From 8 h of PA1 intoxication onwards, we observe several apoptotic epithelial cells with highly condensed cytoplasm and chromatin (Fig. 2G), unfolding of inner mitochondrial membrane (Fig. 2H), and pyknotic nuclei (Fig. 2I). Furthermore, at 12 and 24 h, the presence of membrane-bound apoptotic bodies with well-preserved organelles inside was noted (Fig. 2J and K).

On the other hand, the ultrastructural evaluation also showed necrotic morphological alterations such as mitochondrial swelling with matrix loss, cell swelling with loss of microvilli, rupture of the plasmatic membrane with total or partial loss of cytoplasm, and pyknotic nuclei. These signs were observed at 8 h and increased over time (Fig. 2F, I, L, and O).

3.4. PA1 induces apoptotic histological alterations in the lung

In the lung samples of the ST non-treated and VH control groups, normal histology with epithelial integrity was observed: clean and well-distended alveolar spaces, capillary vessels with erythrocytes in the interalveolar septa, and some collagen fiber stained with H&E and MT (Fig. 3A and B).

At 4 h of PA1 intoxication, nuclei of pneumocytes I and II presented size variability and perinuclear chromatin condensation, some alveolar spaces had hemorrhagic areas, and a light thickening of the interalveolar septum was observed (Fig. 3E and F). At 8 h post-intoxication, we observed chromatin and cytoplasm condensation of pneumocytes I and II, as well as dense hyaline material in the alveolar spaces near the hemorrhagic zones (Fig. 3I and J). At 12 h post-intoxication, lung sections showed increased damage: inflammatory infiltrates composed of polymorphonuclear cells (PMN) and lymphocytes, as well as extensive hemorrhagic zones encompassing the alveolar spaces (Fig. 3M and N).

Finally, at 24 h post-intoxication, apoptotic bodies in pneumocytes I and II (Fig. 3R and S) and hemorrhagic zones with abundant lymphocytes and PMN in the alveolar spaces were observed. At the same time, thickening of the interalveolar septum, fibrosis, exudate, and cellular edema were present.

3.5. PA1 induces ultrastructural alterations of mitochondria in pre-apoptotic and apoptotic pneumocytes

To determine if pre-apoptotic alterations in the lung were present in the short term after treatment, we investigated by TEM the mitochondrial ultrastructure of the pneumocytes. At 4 h, mitochondrial outer membrane rupture and loss of cristae were found in pneumocytes I and II, including hemorrhagic zones in the alveolar spaces and slight thickening of the interalveolar septum with edema in the pneumocyte type I (Fig. 3G and H).

In ultrastructural analysis, we observed that the lungs of the ST group had clean and distended alveolar spaces and the epithelium showed normal morphology: flat cells with flattened nuclei and few organelles in the cytoplasm. The rounded type II pneumocytes had a round nucleus, lamellar bodies, and numerous mitochondria (Fig. 3C and D).

In contrast, in PA1 treated groups at 4, 8, 12, and 24 h post-treatment, thickening of the interalveolar septum of the lungs (Fig. 3G, H, and K), and abundant mitochondrial alterations were

observed. (Fig. 3K, L, O and P). Damage to the alveolar-capillary barrier and apoptotic bodies in pneumocytes I and II was also noted (Fig. 3S and T).

3.6. PA1 induces fragmentation of DNA in kidney and lung

An important step in the apoptosis process is the fragmentation of chromatin controlled by endonucleases, which cleave approximately every 200 base pairs (bp) (Guan et al., 2002). To identify these ruptures, we first performed the TUNEL test, which adds modified nitrogen bases to the ends of the fragmented DNA, revealing the affected cells.

In the histological sections of the kidney of intoxicated mice with PA1, positively stained nuclei were observed after 4 h of treatment (Fig. 4D and E) and were increasing over time (Fig. 4G, H, J, and K). At 24 h, the kidney cortex showed positivity in the epithelial cells of the PCT, DCT, CT as well as in the epithelial cells of the parietal layer of Bowman's capsule and intraglomerular mesangial cells (Fig. 5M). In the medulla, the nuclei of the epithelial cells of the TDT and LH were positive (Fig. 5N). Samples of the non-treated group showed negative results: nuclei stained only with methyl green as a counterstain (Fig. 4A and B). Quantitative analysis of TUNEL-positive cells showed that the cortex of the kidney is most affected at 24 h post-intoxication, when the number of cells is highest (42 ± 7). The other times and quantities were: 12 h (33 ± 5), 8 h (17 ± 4), and 4 h (12 ± 3). We did not observe positive cells in ST and VH control groups. The results reached statistical significance ($P \leq 0.05$, one-way ANOVA) among PA1 treated groups compared to ST control group (Fig. 5C). In the renal medulla, we observed similar results: at 24 h (37 ± 4), 12 h (28 ± 5), 8 h (11 ± 6), and 4 h (7 ± 4). PA1 intoxicated groups showed statistical significance when compared to the ST control group ($P \leq 0.05$, one-way ANOVA) (Fig. 5D).

Likewise, lung samples of the PA1 intoxicated groups at 4, 8, 12, and 24 h of treatment showed positive nuclei in the parenchyma and endothelial cells (Fig. 4F, I, L, and O). It should be noted that numerous nuclei of type I and II pneumocytes, as well as blood cells within capillary vessels, were positive to chromatin fragmentation at 24 h of exposure (Fig. 4O). The histological lung sections of the control groups showed negative results for this technique (Fig. 4C). In quantization of positive cells in lung, we observed at 24 h (18 ± 4), 12 h (12 ± 4), 8 h (8 ± 3), and 4 h (6 ± 2). PA1 intoxicated groups showed statistical significance when compared with the ST control group ($P \leq 0.05$, one-way ANOVA) (Fig. 5E).

As we mentioned previously, among the alterations of cells in apoptosis, the activation of endogenous nucleases cleaves the nuclear DNA at the linkage between nucleosomes, resulting in the production of oligonucleosomal fragments of approximately 200 bp that are identified as an electrophoretic ladder pattern. In our study, we observed that PA1 intoxication induced apoptotic internucleosomal DNA fragmentation in both evaluated organs. DNA ladder pattern was observed at 12 and 24 h, but not at 4 and 8 h post-intoxication in kidney (Fig. 5A). Interestingly, in the kidney, PA1 also caused degradation of genomic DNA. This was observed as a smear pattern that is characteristic of necrotic cell DNA (Fig. 5A). In lung, the electrophoretic ladder pattern was observed only at 24 h post-intoxication (Fig. 5B).

3.7. PA1 induces more DNA fragmentation in the liver than in the kidney and the lung

Finally, we evaluated through spectrophotometry the amount of fragmented DNA in the PA1 target organs at 24 h of treatment. Previously, we demonstrated DNA fragmentation in the liver (Soto-Domínguez et al., 2018); consequently, we compared the induction of apoptosis in all the target organs. Quantitative analysis of fragmented DNA showed that the liver is the most affected organ with the highest percentage ($32.8\% \pm 1.2$), followed by the kidney ($27.2\% \pm 0.7$), and finally the lung ($12.0\% \pm 1.9$). These differences were statistically

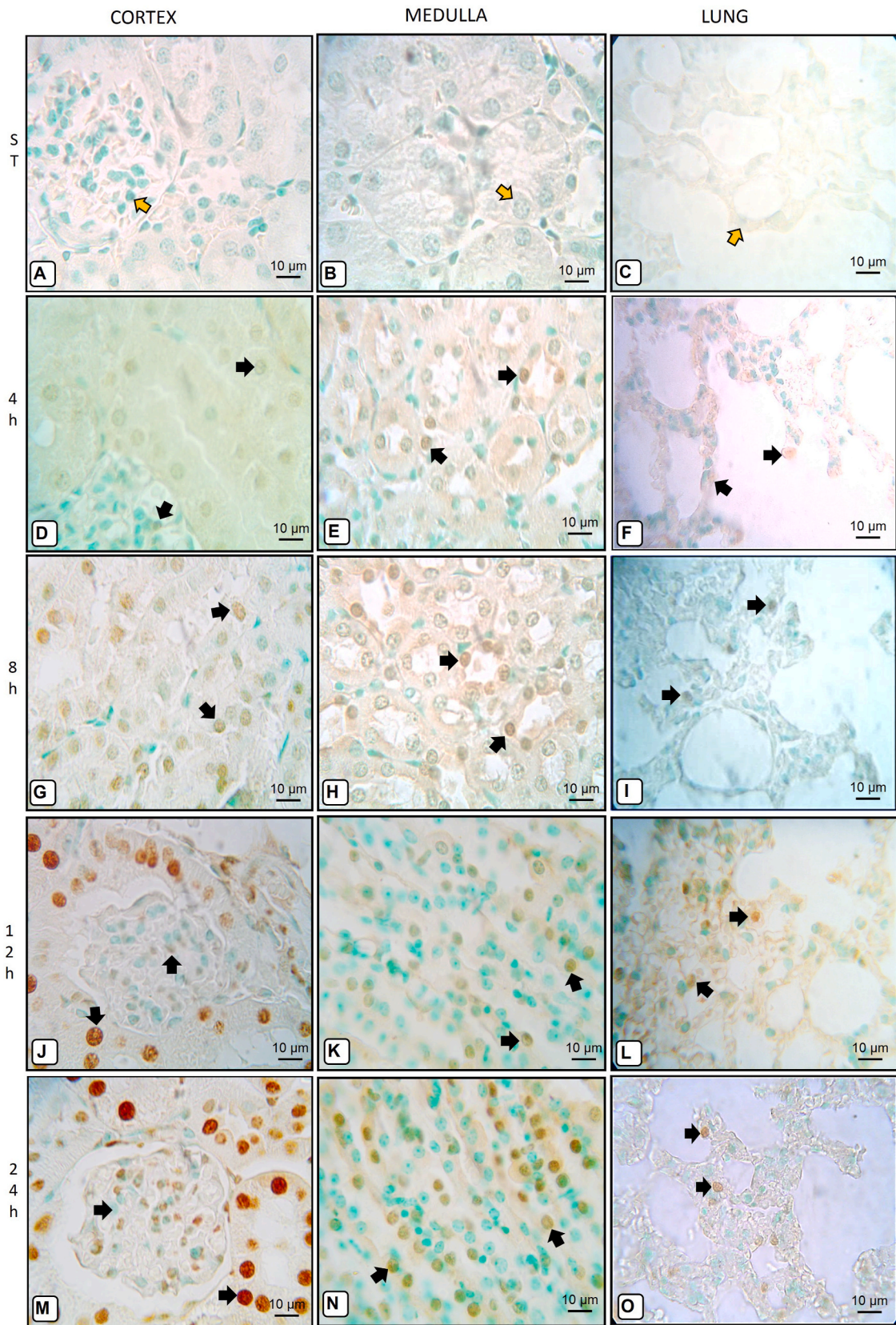


Fig. 4. TUNEL Chromatin fragmentation assay induced by PA1. The non-treated group shows negative nuclei for DNA fragmentation in the renal cortex (A) and medulla (B), as well as in the lung (C). PA1 intoxicated mice at 4 h (D–F); 8 h (G–I); 12 (J–L); and 24 h (M–O) show positive nuclei for DNA fragmentation (black arrows). Scale 10 µm.

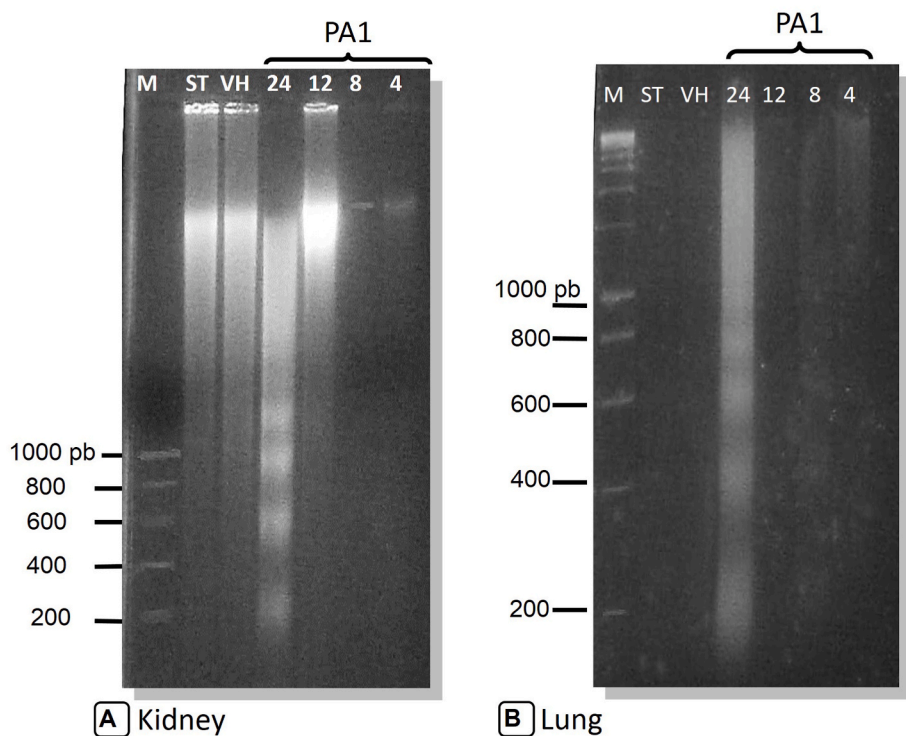
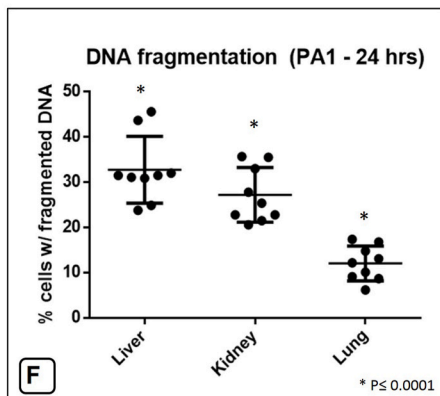
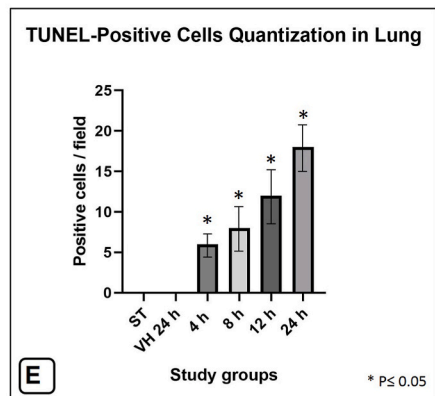
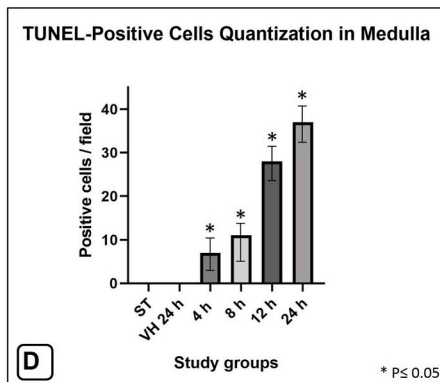
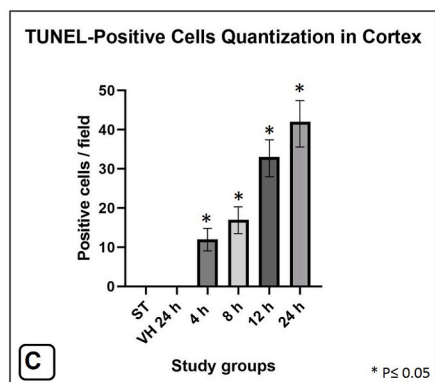


Fig. 5. Identification of fragmented DNA in the kidney and lung by PA1. (A, B) Lane 1–M: Molecular weight marker (DNA ladder); Lane 2–ST: Non-treated group, Lane 3–VH: Safflower oil, Lane 4–PA1 24 h; Lane 5–PA1 12 h; Lane 6–PA1 8 h and Lane 7–PA1 4 h. Observe the ladder pattern. Quantization of TUNEL-positive cells in Cortex (C) and Medulla (D) of the kidney, as well as in lung (E). Statistical significance was reached among PA1 treated groups vs ST control group (* $p \leq 0.05$). F) Quantization of fragmented DNA in liver, kidney, and lung of the group intoxicated with PA1, 24 h of exposure, statistical significance was reached among PA1 treated groups vs ST control group (* $p \leq 0.0001$).



significant ($P < 0.0001$, one-way ANOVA) at 24 h of intoxication (Fig. 5F).

4. Discussion

This study describes for the first time the induction of apoptotic and necrotic alterations in the kidney and lung of mice treated with a toxic

dose of PA1. These findings correlate with previous studies performed in the liver *in vivo* (Soto-Domínguez et al., 2018), and with studies that describe that target organs of this toxin are the liver, kidney, and lung (Bermudez et al., 1986, Bermúdez et al., 1992). In Table 1 we mention some of the studies whose findings correlate with those found in our study.

As apoptosis is a complex process with different proteins and signals

Table 1
Comparative studies with other toxic agents and their effects *in vivo*.

Compound (s)	Organ (s)/ Model	Findings	Reference
Galactosamine (700 mg/kg) i.p. and TNF (10 µg/kg) into the tail vein	Liver of BALB/c mice	Apoptotic death of hepatocytes in galactosamine-sensitized mouse liver after 5 h (TUNEL assay and TEM)	Angermüller et al., 1998
Aminoglycosides in doses of 10–40 mg/kg for 4–10 days	Kidney of Wistar rats	Apoptotic changes (TUNEL assay) were detectable after 4 days of treatment	El Mouedden et al., 2000
Amphotericin B i.p. at 5, 10 and 15 mg/kg/day for 5 consecutive days	Kidney of Sprague Dawley rats	Significant increase and pronounced apoptosis and necrosis in tubular epithelial and mesangial cells (necrotic and apoptotic index), TUNEL and Annexin V assays	Varlam et al., 2001
D-galactosamine (D-GalN)/ lipopolysaccharide (LPS)	Liver of male ICR mice	Hepatocyte apoptosis by histopathological analysis, TUNEL detection, flow cytometry and TEM at 8 h after administering D-GalN/LPS	Wu et al., 2014
PA1 single dose (2LD ₅₀ = 28 mg/kg)	Liver of CD-1 albino mice	Apoptosis by activating the intrinsic mitochondrial apoptotic pathway at 4, 8, 12 and 24 h	Soto-Domínguez et al., 2018
Cisplatin (15 mg/kg)	Kidney of C57BL/6 N mice	Tubular cell apoptosis in kidney cells (TUNEL)	Kim et al., 2019
Aroclor 1254 (10 mg/kg/day) for 15 days	Kidney of male Sprague Dawley rats	Necrosis and hyaline cast in the tubules, apoptotic mesangial and endothelial cells (TEM, TUNEL)	Zeybek et al., 2020
Adenine (0.2% w/w in feed for 4 weeks)	Kidney and lung mice	Lung with polymorphonuclear leukocytes infiltration, injury, and fibrosis. Lipid peroxidation and ROS and decreased of catalase. DNA damage (COMET assay), apoptosis by cleaved caspase-3.	Nemmar A et al., 2017
Mature fruit of <i>K. humboldtiana</i> (3.5 g/kg in 5 doses on days 0, 3, 7, 10 and 14)	Kidney of Wistar rats	Blood vessel congestion, tubular necrosis and fibrosis of renal capsule. Thickening of the filtration barrier and of renal capsule.	García-Garza et al., 2013
Cooper sulfate (CuSO ₄) in drinking water at 100 ppm or 300 ppm during 180 or 300 days.	Aorta and lung of Wistar rats	Vascular damage in the aorta. Active-Caspase-3, and expression of eNOS in the aortic endothelium and endothelium of the capillaries and arterioles of the lung.	Fernández-Rodarte et al., 2022

involved in its development, to date there is no determining test for the detection of apoptosis. Therefore, a series of analyzes should be performed to ensure that the apoptotic process is active or induced. In this study, we used morphological methods for the detection of pre-apoptotic mitochondrial alterations, and the presence of apoptotic bodies within the cells. Also, we applied molecular methods to evaluate the fragmentation of the DNA, and to observe the characteristic ladder DNA pattern of apoptosis.

The mitochondrial alterations reported by Angermüller et al. (1998), appear before the fragmentation of chromatin, and they represent an early marker of the apoptosis process. In the present study, we observed these mitochondrial alterations at 4 h post-intoxication, and we noted an increase over time of chromatin fragmentation and multiple apoptotic bodies. For this reason, it could be considered that the apoptosis process can start quickly, and this may likely be related to the amount of toxin administered in this model.

In the histological and ultrastructural analysis of kidneys in PA1 treated groups, apoptotic mitochondrial alterations and apoptotic bodies were found. However, generalized damage was also observed on the epithelium of the renal tubules with loss of integrity of the basement membrane, loss of the microvilli, pyknotic nuclei, and mitochondria with the loss of the matrix in the epithelial cells after intoxication. These morphological alterations have been reported as markers of necrosis (Searle, 1982).

The kidneys regulate body fluids like urine and participate in the excretion of chemical or toxic products from the bloodstream such as antibiotics, antifungals, antipyretics, or analgesics (Rocha et al., 2001). Some of these compounds and/or their metabolites have been described to cause both apoptosis (El Mouedden et al., 2000; Varlam et al., 2001) and necrosis in the renal parenchyma (Mingeot-Leclercq and Tulkens, 1999), having an important initial effect mainly on the filtration barrier in the glomerulus, intraglomerular mesangial cells, and proximal tubule epithelium. Due to this function, the results obtained in our study suggest a direct effect of the toxin PA1 over the cells of the renal cortex and medulla, resulting in simultaneous activation of apoptosis and necrosis by PA1.

Furthermore, the simultaneous presence of apoptosis and necrosis in renal parenchyma as a response to a single dose of chemical or toxic products in the bloodstream has been reported (Raffray, 1997; El Mouedden et al., 2000; Rocha et al., 2001; Varlam et al., 2001). In our study, we observed both phenomena induced by a single dose of PA1 over the kidney structures.

Likewise, pneumocytes I and II showed mitochondrial pre-apoptotic alterations after 4 h post-intoxication and, subsequently, apoptosis signs and apoptotic bodies. Afterwards, we observed lung edema, abundant cellular infiltrate (mainly PMN and lymphocytes), damage in the alveolus-capillary barrier, and exudate with hemorrhage in the alveolar space. These potent inflammatory effects are most likely associated with necrosis caused by PA1, since pneumocytes II can secrete TNF-α, among other cytokines (Liu et al., 2002), which promote PMN activation and migration, which generate a lesion in the alveolar-capillary barrier (Zimmerman et al., 1983; Sandborg and Smolen, 1988; Chollet-Martin et al., 1994). Also, it has been demonstrated that TNF-α can induce apoptosis by triggering an intracellular cascade that importantly causes mitochondrial changes and the formation of apoptotic bodies (Ding and Yin, 2004); because of these reasons, we suggest that liberation of TNF-α could be involved in the activation of PA1-induced apoptosis in lung parenchyma and blood cells. In our work team it has been described that PA1 causes lung injury characterized by accumulation of PMN cells and lymphocytes trapped in the alveolar capillaries associated with damage to the capillary alveolus barrier, alveolar macrophages, hyaline membrane, and alveolar hemorrhage. Also, an increase in TNF-α in serum and lung at initial times (less than 5 h post-intoxication) was detected, which is correlated with the greater number of PMN cells found in lung injury (Ballesteros-Elizondo, 2000).

The evaluation of DNA fragmentation, visualized as a ladder pattern,

was observed in both organs at 12 and 24 h. Moreover, at 24 h post-treatment a “sweeping” effect was also observed in the kidney, which indicates random DNA degradation attributed to the liberation of lysosomal hydrolytic enzymes in the necrotic process (Ding and Yin, 2004).

The results of the fragmented DNA quantization by spectrophotometry showed that PA1 has a greater effect in the induction of apoptosis in the liver, subsequently in the kidney, and finally in the lung. The induction of apoptosis by PA1 in a higher proportion in the liver could be due to the metabolic effect of this organ on numerous lipophilic compounds (Gyاملani and Parikh, 2002). Furthermore, aromatic toxic compounds and olefinic terpenoids like antracenos can be metabolized to epoxides that induce apoptosis in hepatic cells (Argiriadi et al., 1999; Chen et al., 2001). Previously, we have described that PA1 induces cell death of hepatocytes *in vivo* by triggering the intrinsic apoptotic pathway (Soto-Domínguez et al., 2018). The apoptotic effect could be due to the fact that PA1 is a dimeric anthracenone (Dreyer et al., 1975; Ortega-Martínez et al., 2020), and can be metabolized in the liver to form toxic compounds. These toxic compounds can be sent to the kidney for their excretion, causing damage to this organ, in addition to being in the bloodstream, which can affect the lung.

In conclusion, we demonstrate for the first time that PA1 induces an apoptotic effect in its other target organs: kidney and lung. Although, this effect has a variable intensity between target organs, and kidney necrosis is also activated later. These results can help in the understanding of the mechanism of action of this compound at toxic doses *in vivo*.

Credit author statement

Adolfo Soto-Domínguez: Conceptualization, Methodology, Resources, Writing & Reviewing the original and final draft. **Daniel Salas-Treviño:** Methodology, Validation, Writing & reviewing the original and final draft. **Gloria A. Guillén-Meléndez:** Writing & reviewing final draft. **Uziel Castillo-Velázquez:** Writing & reviewing the original and final draft. **Raquel G. Ballesteros-Elizondo:** Conceptualization, Methodology, Validation, Formal Analysis, Resources. **Sheila A. Villacédillo:** Writing & reviewing final draft. **Rodolfo Morales-Ávalos:** Writing & reviewing the original draft. **Luis E. Rodríguez-Tovar:** Writing & reviewing the original draft. **Roberto Montes-de-Oca-Luna:** Validation, Methodology, Resources, Writing & reviewing the original and final draft. **Carlos R. Montes-de-Oca-Saucedo:** Reviewing final draft. **Odila Saucedo-Cárdenas:** Conceptualization, Methodology, Validation, Resources, Writing & reviewing the original and final draft.

Ethical statement

All the animals were kept under standard laboratory conditions, experiments were performed according to the International Guidelines on the Appropriate Use of Experimental Animals, and according to Mexican Norm NOM-062-ZOO-1999 on the Technical Specifications for Production, Care and Use of Laboratory Animals.

Declaration of competing interest

The authors declare that they have no known competing financial interests or personal relationships that could have appeared to influence the work reported in this paper.

Data availability

No data was used for the research described in the article.

Acknowledgment

This study was partially supported by PROMEP-SEP-México grant 103.5/04/757. Adolfo Soto Domínguez was a scholarship recipient of

CONACyT (Consejo Nacional de Ciencia y Tecnología), Mexico scholarship 171880. We acknowledge the work of QCB Rosa Maria Leal for the technical assistance involved in processing the samples for TEM. The present study is dedicated to the memory of Ph. D. Julio Sepúlveda-Saavedra (†February 10th, 2014), Chairman of the Histology Department, Faculty of Medicine, UANL until the day of his death.

References

- Angermüller, S., Künstle, G., Tieg, G., 1998. Pre-apoptotic Alterations in hepatocytes of TNF α -treated galactosamine-sensitized mice. *J. Histochem. Cytochem.* 46 (10), 1175–1183. <https://doi.org/10.1177/002215549804601009>.
- Argiriadi, M.A., Morisseau, C., Hammock, B.D., Christianson, D.W., 1999. Detoxification of environmental mutagens and carcinogens: structure, mechanism, and evolution of liver epoxide hydrolase. *Proc. Natl. Acad. Sci. USA* 96 (19), 10637–10642.
- Ballesteros Elizondo Raquel Guadalupe, 2000. Factor de Necrosis Tumoral y granulocitos neutrófilos en la producción del síndrome de insuficiencia respiratoria del adulto causado por Peroxisomicina A-1. Tesis Doctoral. Tumor Necrosis Factor and neutrophilic granulocytes in the production of adult respiratory distress syndrome caused by Peroxisomicine A1, Doctoral Thesis. <http://cdigital.dgb.uanl.mx/te/1080111678/1080111678.html>. Accessed on August 5, 2021.
- Bermudez, M.V., Gonzalez-Spencer, D., Guerrero, M., Waksman, N., Piñeyro, A., 1986. Experimental intoxication with fruit and purified toxins of buckthorn (*Karwinskia humboldtiana*). *Toxicol* 24 (11), 1091–1097. [https://doi.org/10.1016/0041-0101\(86\)90135-2](https://doi.org/10.1016/0041-0101(86)90135-2).
- Bermúdez, M.V., Martínez, F.J., Salazar, M.E., Waksman, N., Piñeyro, A., 1992. Experimental acute intoxication with ripe fruit of *Karwinskia humboldtiana* (Tullidora) in rat, Guinea-pig, hamster and dog. *Toxicol* 30 (11), 1493–1496. [https://doi.org/10.1016/0041-0101\(92\)90527-C](https://doi.org/10.1016/0041-0101(92)90527-C).
- Burton, K., 1956. A study of the conditions and mechanism of the diphenylamine reaction for the colorimetric estimation of deoxyribonucleic acid. *Biochem. J.* 62 (2), 315–323. <https://doi.org/10.1042/bj0620315>.
- Chen, J.-K., Capdevila, J., Harris, R.C., 2001. Cytochrome p450 epoxygenase metabolism of arachidonic acid inhibits apoptosis. *Mol. Cell Biol.* 21 (18), 6322–6331.
- Chollet-Martin, S., Montravers, P., Gibert, C., et al., 1994. Relationships between polymorphonuclear neutrophils and cytokines in patients with adult respiratory distress syndrome. *Ann. N. Y. Acad. Sci.* 725 (1), 354–366.
- Ding, W., Yin, X., 2004. Dissection of the multiple mechanisms of TNF- α -induced apoptosis in liver injury. *J. Cell Mol. Med.* 8 (4), 445–454.
- Dreyer, D.L., Arai, I., Bachman, C.D., Anderson, W.R., Smith, R.G., Daves, G.D., 1975. Toxins causing noninflammatory paralytic neuropathy. Isolation and structure elucidation. *J. Am. Chem. Soc.* 97 (17), 4985–4990. <https://doi.org/10.1021/ja00850a037>.
- El Mouedden, M., Laurent, G., Mingeot-Leclercq, M.-P., Taper, H.S., Cumps, J., Tulkens, P.M., 2000. Apoptosis in renal proximal tubules of rats treated with low doses of aminoglycosides. *Antimicrob. Agents Chemother.* 44 (3), 665–675.
- Fernández-Rodarte, B.A., Soto-Domínguez, A., González-Navarro, A., Mellado-Ayala, A., Piña-Mendoza, E.I., Rodríguez-Rocha, H., Montes-De-Oca-Luna, R., Guerra-Leal, J. D., Guzmán-López, S., Elizondo-Omaña, R.E., 2022. Copper induces damage, oxidative stress and cell death in endothelium of chronic intoxicated Wistar rats. *Int. J. Morphol.* 40 (1), 10–17, 2022.
- García, G.R., Salazar, L.M.E., Romero, D.V., García, J.J., Soto, D.A., Juárez, R.O.A., Sepúlveda, S.J., 2013. Chronic intoxication with ripe fruit of *Karwinskia humboldtiana* in wistar rats: renal damage. *Int. J. Morphol.* 31 (4), 1449–1454.
- Gendimenico, G.J., Bouquin, P.L., Tramosch, K.M., 1988. Diphenylamine-colorimetric method for DNA assay: a shortened procedure by incubating samples at 50°C. *Anal. Biochem.* 173 (1), 45–48. [https://doi.org/10.1016/0003-2697\(88\)90156-X](https://doi.org/10.1016/0003-2697(88)90156-X).
- Guan, J., Jin, L., Lu, Q., 2002. Apoptosis in organs of rats in early stage after polytrauma combined with shock. *J. Trauma Acute Care Surg* 52 (1), 104–111.
- Guerrero, M., Piñeyro, A., Waksman, N., 1987. Extraction and quantification of toxins from *Karwinskia humboldtiana* (Tullidora). *Toxicol* 25 (5), 565–568. [https://doi.org/10.1016/0041-0101\(87\)90292-3](https://doi.org/10.1016/0041-0101(87)90292-3).
- Gyاملani, G.G., Parikh, C.R., 2002. Acetaminophen toxicity: suicidal vs accidental. *Crit. Care* 6 (2), 155.
- Ito, S., 1968. Formaldehyde-glutaraldehyde fixatives containing trinitro compounds. *J. Cell Biol.* 39, 168A.
- Kerr, R.J.F., 1994. Morphological criteria for identifying apoptosis. *Cell Biol.* 1, 319–329. <http://ci.nii.ac.jp/naid/10018531553/en/>. Accessed October 21, 2019.
- Kerr, J.F.R., Wyllie, A.H., Currie, A.R., 1972. Apoptosis: a basic biological phenomenon with wideranging implications in tissue kinetics. *Br. J. Cancer* 26 (4), 239–257. <https://doi.org/10.1038/bjc.1972.33>.
- Kerr, J.F.R., Góbe, G.C., Winterford, C.M., Harmon, B.V., 1995. Chapter 1 Anatomical Methods in Cell Death. In: Schwartz, L.M., Osborne BABT-M in, C.B. (Eds.), *Cell Death*, vol. 46. Academic Press, pp. 1–27. [https://doi.org/10.1016/S0091-679X\(08\)61921-4](https://doi.org/10.1016/S0091-679X(08)61921-4).
- Kim, J.W., Jo, J., Kim, J.Y., Choe, M., Leem, J., Park, J.H., 2019. Melatonin attenuates cisplatin-induced acute kidney injury through dual suppression of apoptosis and necroptosis. *Biology* 8 (3), 64. <https://doi.org/10.3390/biology8030064>.
- Lansiaux, A., Laine, W., Baldeyrou, B., et al., 2001. DNA topoisomerase II inhibition by peroxisomicine A1 and its radical metabolite induces apoptotic cell death of HL-60 and HL-60/MX2 human leukemia cells. *Chem. Res. Toxicol.* 14 (1), 16–24. <https://doi.org/10.1021/tx000145j>.

- Liu, M., 2002. In: Baue, A.E., Berlot, G., Gullo, A., Vincent, J.-L. (Eds.), *Alveolar Epithelium in Host Defence: Cytokine Production BT - Sepsis and Organ Dysfunction*. Springer Milan, Milano, pp. 37–50.
- Majno, G., Joris, I., 1995. Apoptosis, oncosis, and necrosis. An overview of cell death. *Am. J. Pathol.* 146 (1), 3–15. <https://www.ncbi.nlm.nih.gov/pubmed/7856735>.
- Martínez, F.J., Zeng, G.-Q., Piñeyro, A., Garza-Ocañas, L., Tomei, L.D., Umansky, S.R., 2001. Apoptosis induction and cell cycle perturbation in established cell lines by peroxisomicine A1 (T-514). *Drug Chem. Toxicol.* 24 (3), 287–299. <https://doi.org/10.1081/DCT-100103725>.
- Mingeot-Leclercq, M.-P., Tulkens, P.M., 1999. Aminoglycosides: nephrotoxicity. *Antimicrob. Agents Chemother.* 43 (5), 1003–1012.
- Nemmar, A., Karaca, T., Beegam, S., Yuvaraju, P., Yasin, J., Ali, B.H., 2017. Lung oxidative stress, DNA damage, apoptosis, and fibrosis in adenine-induced chronic kidney disease in mice. *Front. Physiol.* 8, 896. <https://doi.org/10.3389/fphys.2017.00896>. Nov 23 PMID: 29218013; PMCID: PMC5703828.
- Ortega-Martínez, M., Gutiérrez-Dávila, V., Niderhauser-García, A., Salazar-Aranda, R., Solís-Soto, J.M., Montes-De-Oca-Luna, R., Jaramillo-Rangel, G., 2020. Peroxisomicine A1, a potential antineoplastic agent, causes micropexophagy in addition to macropexophagy. *Cell Biol. Int.* 44, 918–923.
- Piñeyro-López, A., de Villarreal, L.M., González-Alanís, R., 1994. *In vitro* selective toxicity of toxin T-514 from *Karwinskia humboldtiana* (buckthorn) plant on various human tumor cell lines. *Toxicology* 92 (1), 217–227. [https://doi.org/10.1016/0300-483X\(94\)90179-1](https://doi.org/10.1016/0300-483X(94)90179-1).
- Raffray, M., 1997. Apoptosis and necrosis in toxicology: a continuum or distinct modes of cell death? *Pharmacol. Ther.* 75 (3), 153–177.
- Rocha, G.M., Michea, L.F., Peters, E.M., et al., 2001. Direct toxicity of nonsteroidal antiinflammatory drugs for renal medullary cells. *Proc. Natl. Acad. Sci. USA* 98 (9), 5317–5322.
- Sandborg, R.R., Smolen, J.E., 1988. Early biochemical events in leukocyte activation. *Lab. Invest.* 59 (3), 300–320.
- Searle, J., 1982. Necrosis and apoptosis: distinct modes of cell death with fundamentally different significance. *Pathol. Annu.* 17 (2), 229–259.
- Sepúlveda Saavedra, J., van der Klei, I.J., Keizer, I., Lopez, A.P., Harder, W., Veenhuis, M., 1992. Studies on the effect of toxin T-514 on the integrity of peroxisomes in methylotrophic yeasts. *FEMS Microbiol. Lett.* 91 (3), 207–212. <https://doi.org/10.1111/j.1574-6968.1992.tb05210.x>.
- Soto-Domínguez, A., Piñeyro-López, A., Saucedo-Cárdenas, O., Ramírez-Durón, R., Waksman de Torres, N., Sepúlveda-Saavedra, J., 2012. Early administration of peroxisomicine A1 (T-514 extracted from *K. parvifolia* seeds) causes necrosis of implanted TC-1 cells without affecting target organs in a murine model. *Int. J. Morphol.* 30 (1), 284–289. <https://doi.org/10.4067/s0717-95022012000100051>.
- Soto-Domínguez, A., Ballesteros-Elizondo, R.G., Santoyo-Pérez, M.E., et al., 2018. Peroxisomicine A1 (toxin T-514) induces cell death of hepatocytes *in vivo* by triggering the intrinsic apoptotic pathway. *Toxicon* 154, 79–89. <https://doi.org/10.1016/j.toxicon.2018.09.010>.
- Varlam, D.E., Siddiq, M.M., Parton, L.A., Rüssmann, H., 2001. Apoptosis contributes to amphotericin B-induced nephrotoxicity. *Antimicrob. Agents Chemother.* 45 (3), 679–685.
- Waksman de Torres, N., Ramirez Duran, R., 1992. Isolation of a new dimeric anthracenone from *Karwinskia parvifolia*. *Rev. Latinoam. Quim.* 22, 25.
- Wu, Y., Hu, S., Liu, J., Cao, H., Xu, W., Li, Y., Li, L., 2014. Nature and mechanisms of hepatocyte apoptosis induced by D-galactosamine/lipopolysaccharide challenge in mice. *Int. J. Mol. Med.* 33, 1498–1506. <https://doi.org/10.3892/ijmm.2014.1730>.
- Zeybek, N.D., Sur, Ü., Oflaz, O., Erkekoğlu, P., Balci, A., Özkemahlı, G., Aşçı, A., Kızılgün, M., Edebal, O.H., Koçer-Gümüşel, B., 2020. Renal changes and apoptosis caused by subacute exposure to Aroclor 1254 in selenium-deficient and selenium-supplemented rats. *Arh. Hig. Rad. Toksikol.* 71 (2), 110–120. <https://doi.org/10.2478/aiht-2020-71-3360>.
- Zimmerman, G.A., Renzetti, A.D., Hill, H.R., 1983. Functional and metabolic activity of granulocytes from patients with adult respiratory distress syndrome: evidence for activated neutrophils in the pulmonary circulation. *Am. Rev. Respir. Dis.* 127 (3), 290–300.